The results shown in the figure are the best obtained for these particular designs. Discrepancy between theory and experiment is expected because i) the theory does not account for loss, ii) the method of obtaining the experimental eigenvalues from the measurements assumes there is no loss, and iii) only a finite number of modes is included (e.g., for $\lambda_0$ for the 2-port with a disk, $K=2$, $M=4$ means that the azimuthal spacial frequencies accounted for are 0, $\pm 2$, $\pm 4$ ($= \pm gK$), and in the $z$-direction modes with up to four half-wavelengths are included). However, the correlation is very good.

For the 2-port case it is seen that the disk has a greater influence on $\lambda_0$ than on $\lambda_1$. This is to be expected since the disk is of small radius and the stationary (for $\lambda_0$) and the rotating (for $\lambda_1$) junction modes have high and low electric fields near the junction center. For the 3-port the disk has little effect on $\lambda_0$. This suggests the edge of the disk is in a region of low electric field. Indeed, the disk and no-disk cases give the same result at 11 GHz and it is found that the first root of $J_0(\omega\sqrt{\mu_0\epsilon_0}\, r)$ gives the result $r = 10.4$ mm: the disk radius is 10.0 mm. For the rotating junction made the dominant field mode Bessel function, $J_1$, is near a maximum for the whole frequency band at the disk edge. This means that the electric field is high and, therefore, a high value of $M$ is required for accurate results. It is, therefore, not surprising that errors as large as 22° occur in this case. Also, this particular eigenvalue is degenerate, i.e., $\lambda_1 = \lambda_2$, and numerical errors are expected in such cases [1], although the results for the case of no-disk are very good.

## IX. Conclusions

An exact three-dimensional field theory has been formulated for a class of cyclic $H$-plane waveguide junction, and a small number of designs have been briefly evaluated to test the theory. The accuracy of the results is very good, thus indicating the theory is valid and has been programmed correctly. The problem solved here has involved the organization of a large number of linear simultaneous equations with the aid of matrix notation. The inclusion of extra dielectric or ferrite regions can be achieved by defining the appropriate matrices and including them in the matrix product occurring in the theory. Additional metal disks can also be included by introducing the appropriate matrices. Thus the method developed in this paper represents a principle for dealing with a multistep pedestal, multidielectric, multiferrite-loaded junction, with or without a central metal pin.

## References

[1] J. B. Davies, "An analysis of the $m$-port symmetrical $H$-plane waveguide junction with central ferrite post," *IRE Trans. Microwave Theory Tech.*, vol. MTT-10, pp. 596–604, Nov. 1962.

[2] M. E. El-Shandwily *et al.*, "General field theory treatment of $H$-plane waveguide junction circulators," *IEEE Trans. Microwave Theory Tech.*, vol. MTT-21, pp. 392–403, June 1973.

[3] ——, "General field theory treatment of $E$-plane waveguide junction circulators–Part II: Two-disk ferrite configuration," *IEEE Trans. Microwave Theory Tech.*, vol. MTT-25, pp. 794–803, Sept. 1977.

[4] J. A. Stratton, *Electromagnetic Theory*. New York: McGraw-Hill, 1941.

[5] M. Abramowitz and I. A. Stegun, *Handbook of Mathematical Functions*, Dover, New York, 1965.

# On the Modeling of the Edge-Guided Mode Stripline Isolators

SALVADOR H. TALISA, MEMBER, IEEE, AND DONALD M. BOLLE, SENIOR MEMBER, IEEE

***Abstract*—A model for the inhomogeneously ferrite-loaded microstrip and stripline is considered. The structure consists of a loaded ferrite slab between two infinite, perfectly conducting planes with the bias magnetization perpendicular to the ground planes. The ferrite is taken to be lossy and is loaded on one side by a semi-infinite lossy material and on the other by a dielectric slab. The modal spectrum of this configuration as well as the influence on the $\omega$-$\alpha$ and $\omega$-$\beta$ diagrams of the various parameters involved are studied. Special attention has been paid to the capabilities of this configuration to model a nonreciprocal isolator. A hypothetical isolator is designed, and its characteristics are compared with experimental results obtained by Hines, Dydyk, and Courtois. Substantial agreement is observed.**

Manuscript received July 10, 1978; revised December 6, 1978.

The authors are with the Division of Engineering, Brown University, Providence, RI 02912.

## I. Introduction

An investigation of edge-guided waves propagating in ferrite-loaded strip and microstriplines magnetized perpendicular to the ground plane was initiated by Hines [1]–[3] in the late 1960's. Hines deduced that the dominant mode propagating through such struc-

0018-9480/79/0600-0584$00.75 ©1979 IEEE

tures resembled a TEM mode. Furthermore, a strong field displacement effect was observed, through which the propagated wave energy concentrates along one of the edges of the transmission line.

For a sufficiently wide conducting strip, the problem was approached analytically [2] by neglecting the effect of the fringing fields as a first approximation. Thus a vertical perfect magnetic wall boundary condition could be imposed at the edges of the conducting strip. The nonreciprocal transverse field displacement effect was enhanced by asymmetrically loading the edges of the transmission line. Experimental prototypes for isolators, phase-shifters [1], [2], and circulators [3] were developed.

The potential which the edge-guided waves offered for the development of broad-band ferrite substrate microwave integrated-circuit components induced several researchers in Europe, Japan, and America to engage in the task of achieving a more complete understanding of these modes and their possible applications.

Workers like Courtois and deSantis at first approached the study of the edge-guided mode through the analysis of the related surface waves in simple geometries such as a ferrite–dielectric interface [4], [5], with the bias magnetization parallel to the interface and normal to the propagation direction. It was then discovered that two different unidirectional surface modes could propagate through such a structure according to the direction of propagation (or the sign of the dc magnetizing field), i.e., the dynamic and magnetostatic modes, respectively. The latter can only propagate at those frequencies for which the ferrite effective permeability $\mu_{\text{eff}}$ is negative ($\gamma\sqrt{HB} < \omega < \gamma B$). However, the dynamic mode has the same lower cutoff as the magnetostatic mode ($\omega = \gamma\sqrt{HB}$) but extends beyond the frequency for which $\mu_{\text{eff}}$ becomes positive, up to the point where, on the dispersion diagram, it intersects the curve $\omega\sqrt{\epsilon_f \epsilon_0 \mu_{\text{eff}}}$, where $\epsilon_f$ is the relative permittivity of the ferrite.

Analyses of different models which successively approach actual ferrite-loaded microstrip and stripline structures followed. Good examples of this can be found in the work by Courtois *et al.* [6], [7], deSantis [8]–[10], and Bolle [11]–[15]. In passing from the ferrite half-space model to a finite-width ferrite slab in a dielectric medium or a ferrite slab between perfect magnetic walls, the unidirectional surface waves transformed into surface modes displaying a nonreciprocal transverse field displacement effect. It was found that for the dynamic and magnetostatic modes, the energy is concentrated near opposite faces of the ferrite slab for the same direction of propagation.

With regard to specific edge-guided mode devices, the work on isolators by Courtois [16]–[18] and Dydyk [19] is of particular interest to us. The model basic to this study consists of a ferrite slab, sided by dielectric, between two infinite perfectly conducting planes. The magnetization was taken to be normal to the ground planes. The effect of the fringing fields in an actual microstrip or stripline structure, therefore, is neglected.

The analysis of such a configuration is extended to include either a semi-infinite lossy medium or a lossy film interspersed between one side of the ferrite slab and the dielectric region, while on the other side a dielectric slab is placed whose permittivity differs from that of the surrounding medium. An exact solution of the model containing a semi-infinite lossy region will be treated here (Fig. 1). The results for the resistive film will be reported in a forthcoming publication.

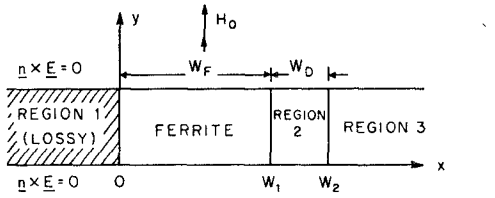


Fig. 1. Canonical stripline geometry for the semi-infinite lossy region model.

The presence of losses implies not only a quantitative complication but also a mathematical one, for now the dispersion relation and the field expressions are complex functions of a complex variable, i.e., the propagation constant. Thus the main difficulty which appears in the treatment of these problems is the detection and distinguishing between the propagation constants of different modes which arise out of the dispersion relations.

These relations are somewhat complicated transcendental equations and can only be solved using numerical methods. Thus a special subroutine (ZSYSTM) from the IMSL library [20] employing Brown's method [21], [22] was used. Whenever convergence was difficult to achieve, an electronic plotter was used to visualize the form of the dispersion relation, so as to choose suitable starting values for the iterative loop. Results are obtained which show the forward and reverse dispersion characteristics for different values of the various parameters involved.

Special attention has been paid to the dynamic and magnetostatic modes as well as to the first higher order mode. The results obtained reflect on the utility which this structure may have in modeling nonreciprocal broad-band isolators using the field displacement effect. In this respect, an optimum design of an isolator is attempted, and its characteristics are compared with the experimental results obtained by Hines [2], Forterre *et al.* [17], and Dydyk [19]. Overall agreement is obtained. Some differences between our dispersion diagrams and those reported by Forterre in [17] concerning the forms of the dynamic and first higher order modes are also discussed.

## II. Theory

The geometry to be analyzed is shown in Fig. 1 where the shaded area, region 1, represents the semi-infinite lossy region. It extends to $x \to -\infty$, while region 3 extends to $x \to +\infty$. Region 2 is a dielectric slab with a permittivity which differs in general from that of regions 1 and 3.

For a magnetizing field $H_0$ taken perpendicular to the ground planes, the permeability tensor takes the form

TABLE I

| | |
|---|---|
| $\omega$ = angular frequency (rad/s) | $\mu_0$ = vacuum permeability |
| $H_0$ = dc magnetizing field (oersteds) | $=4\pi\times10^{-7}$ H/m |
| $\Delta H_0$ = ferrite resonance line width (oersteds) | $\omega_0=\gamma_0(H_0+j\frac{\Delta H_0}{2})$ |
| $4\pi M_s$ = saturation magnetization (gauss) | $\omega_m=\gamma_0 4\pi M_s$ |
| $\gamma_0$ = gyromagnetic ratio | $\chi=\frac{\omega_0\omega_m}{\omega_0^2-\omega^2}$ |
| $=1.76\times10^7$ rad/(s·Oe) | $\kappa=\frac{-\omega\omega_m}{\omega_0^2-\omega^2}$ |

$$\underline{\underline{\mu}}=\mu_0\begin{vmatrix}1+\chi & 0 & j\kappa\\ 0 & 1 & 0\\ -j\kappa & 0 & 1+\chi\end{vmatrix}.$$

The different parameters involved in this matrix are listed in Table I.

We restrict our consideration to the lowest order TE modes. In addition, we will only consider the case of no variation in the $y$ direction. Under these restrictions only three field components result: $E_y$, $H_x$, and $H_z$.

The electric field component $E_y$ satisfies second-order wave equations in all regions of Fig. 1. In solving these wave equations we have taken $e^{j\omega t}$ and $e^{-\gamma z}$ as the time-dependent and the propagation factors, respectively. The propagation constant $\gamma=\alpha+j\beta$ has its real and imaginary parts positive for propagation in the positive $z$ direction. Thus in each of the four regions of Fig. 1 the solution to the wave equation is, in general, of the form

$$E_y=(C_1e^{Qx}+C_2e^{-Qx})e^{j\omega t-\gamma z}. \tag{1}$$

The expressions for $H_x$ and $H_z$ as a function of $E_y$ are readily obtained from Maxwell's equations.

Application of the boundary conditions will give us a homogeneous linear system of six equations in six unknowns, i.e.,

$$[D]\cdot[C]=0 \tag{2}$$

where $[D]$ is a six-by-six matrix whose elements are functions of $\omega$ and $\gamma$ and $[C]$ is a column vector formed by six unknown elements equivalent to the constants $C_i$ for the various regions.

For a nontrivial solution, the determinant of the matrix of coefficients must vanish, thus giving a transcendental equation in $\omega$ and $\gamma$ of the form

$$F(\omega,\gamma)=\tan kW_F - \frac{D_1(\omega,\gamma)\sin k_2W_D+D_2(\omega,\gamma)\cos k_2W_D}{D_3(\omega,\gamma)\sin k_2W_D+D_4(\omega,\gamma)\cos k_2W_D}=0 \tag{3}$$

where $W_F$ and $W_D$ are the ferrite and dielectric slab widths, respectively, and

$$D_1(\omega,\gamma)=\frac{k\mu_{\text{eff}}}{k_2}(k_2^2+k_{1L}k_1)$$

$$D_2(\omega,\gamma)=jk\mu_{\text{eff}}(k_1+k_{1L})$$

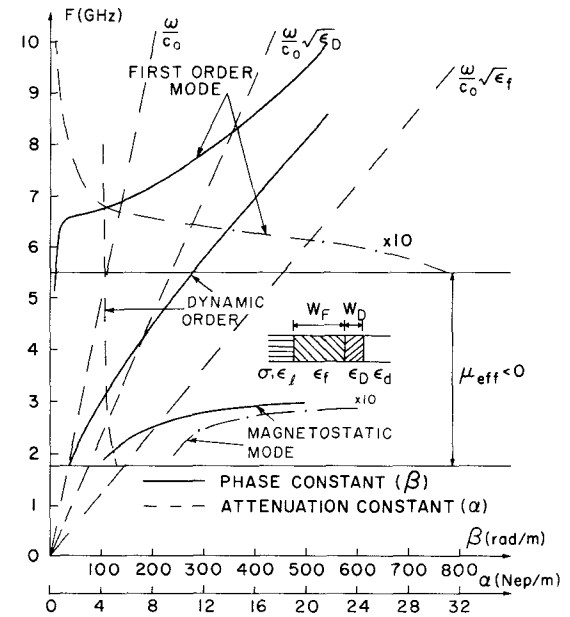


Fig. 2. Dispersion characteristics and attenuation constants for different modes corresponding to a geometry as in the inset. Forward propagation. Parameters: $4\pi M_s=1760$ G, $H_0=200$ Oe, $\Delta H_0=90$ Oe, $\sigma=1.0$ mho/m, $W_F=10$ mm, $\epsilon_f=15$, $W_D=2$ mm, $\epsilon_D=4$, $\epsilon_l=\epsilon_d=1$.

$$D_3(\omega,\gamma)=j\left[\left(k_{1L}\mu_{\text{eff}}+\frac{\gamma\kappa}{1+\chi}\right)\left(k_2\mu_{\text{eff}}-\frac{k_1}{k_2}\frac{\gamma\kappa}{1+\chi}\right)+\frac{k_1k^2}{k_2}\right]$$

$$D_4(\omega,\gamma)=\left(k_{1L}\mu_{\text{eff}}+\frac{\gamma\kappa}{1+\chi}\right)\left(\frac{\gamma\kappa}{1+\chi}-k_1\mu_{\text{eff}}\right)-k^2$$

with

$$\mu_{\text{eff}}=1+\chi-\frac{\kappa^2}{1+\chi}$$

$$k_{1L}^2=\gamma^2+\omega^2\mu_0\left(\epsilon_l\epsilon_0-j\frac{\sigma}{\omega}\right)$$

$$k_1^2=\gamma^2+\omega^2\mu_0\epsilon_d\epsilon_0$$

$$k^2=\gamma^2+\omega^2\epsilon_0\epsilon_f\mu_{\text{eff}}\mu_0$$

$$k_2^2=\gamma^2+\omega^2\epsilon_0\epsilon_D\mu_0.$$

The following notation has been used.

| | |
|---|---|
| $\mu_{\text{eff}}\equiv$ effective ferrite permeability | $\epsilon_d\equiv$ relative permittivity of the semi-infinite dielectric medium (region 3, Fig. 1) |
| $\epsilon_0,\mu_0\equiv$ vacuum permittivity and permeability, respectively | |
| $\epsilon_l\equiv$ relative permittivity of the lossy medium | $\epsilon_f\equiv$ ferrite relative permittivity |
| $\sigma\equiv$ conductivity of the lossy medium | $\epsilon_D\equiv$ dielectric slab relative permittivity |

Taking $\omega$ as a parameter, the solution $\gamma$ of (3) is approached by using numerical techniques. The subroutine ZSYSTM from the IMSL library [20] was employed. ZSYSTM is designed to solve $N$ simultaneous nonlinear equations in $N$ unknowns. In our case, $N=2$, and the two equations are the real and imaginary parts of $F(\omega,\gamma)$ both equated to zero. The two variables are the real and imaginary parts of $\gamma$. The method used by ZSYSTM is described in [21] and [22].

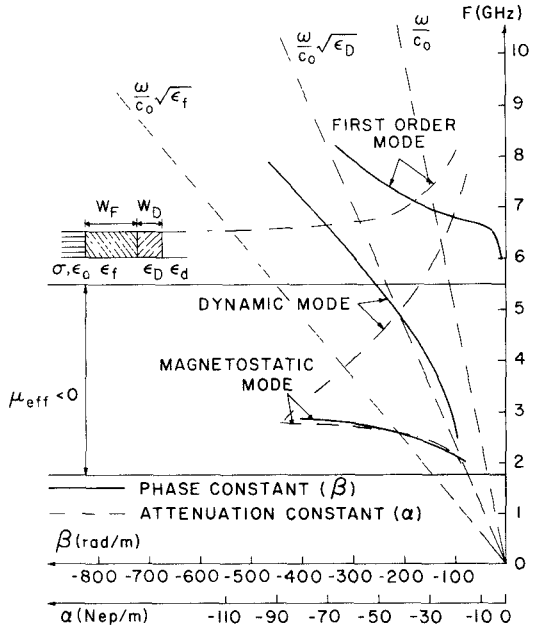


Fig. 3. Dispersion characteristics and attenuation constants for the reverse propagation. Parameters as for Fig. 2.

Once the propagation constant $\gamma$ is obtained from (3), we use (2) to obtain five of the elements of $[C]$ as a function of the sixth one which can be assigned any arbitrary value. We thus obtain the amplitudes of the field components which may be plotted to allow inspection of the modal structure.

Summarizing, we have available a computer program which for a given frequency $\omega$, gives propagation constants ($\gamma$) for particular modes of propagation and plots the field components as a function of the transverse coordinate $x$.

## III. Results

Before we begin a detailed discussion of the results, some general remarks must be made. For this purpose we will refer to Figs. 2 and 3 which represent, respectively, the forward and reverse dispersion diagrams—along with the attenuation constants for each mode for the model shown in the inset of the figures. The different parameters involved were defined before and their values are

| | |
|---|---|
| $4\pi M_s = 1760$ gauss | $\epsilon_f = 15$ |
| $H_0 = 200$ Oe | $W_D = 2$ mm |
| $\Delta H_0 = 90$ Oe | $\epsilon_D = 4$ |
| $\sigma = 1.0$ mho/m | $\epsilon_l = 1$ |
| $W_F = 10$ mm | $\epsilon_d = 1$. |

The values of $4\pi M_s$ and $\epsilon_f$, as well as the bias magnetization given above, were chosen to be the same as in [14], [15], and [13, part II], so as to allow direct comparison between the results.

In Fig. 2 we observe the following modes.

1) The waveguide (dynamic) mode which is restricted to the region between the line whose slopes are the phase velocity of plane waves in a vacuum (since $\epsilon_l = \epsilon_d = 1$) and in a dielectric medium with dielectric constant $\epsilon_f$.

2) The surface (magnetostatic) mode, restricted to the region where $\mu_{eff} < 0$.

3) The first higher order mode. (The volume modes, below the region where $\mu_{eff} < 0$, have been neglected.)

The dynamic and magnetostatic modes are characterized by a concentration of the propagated energy in the vicinity of one or the other face of the ferrite slab. This is the so-called field displacement effect. For the case of Fig. 1, in the dynamic mode the energy adheres to the right-hand side of the ferrite slab as the fields propagate in the positive $z$ direction. The magnetostatic mode propagates near the opposite face and consequently suffers attenuation due to the lossy region. The degree of attenuation will depend on the loss parameter. The opposite effect occurs for propagation in the reverse direction.

Figs. 2 and 3 illustrate this. The forward dynamic attenuation constant or insertion loss is very low compared to the attenuations of the surface and first-order modes. On the contrary, for the reverse propagation the dynamic attenuation constant or isolation is higher or comparable to the one corresponding to the magnetostatic mode in the range of frequencies where they overlap. The first-order mode attenuation constant is of the same order of magnitude for both forward and reverse propagations.

In contrast with the magnetostatic mode, the dynamic mode shows the field displacement effect for a much wider range of frequencies, as has previously been noted in [13]–[15]. To utilize fully this property of the dynamic mode, one must take into account that its effective bandwidth is limited above by the onset of the first higher order mode and below by the onset of the magnetostatic mode. Thus operation within the range of either of these is not advisible unless they are sufficiently attenuated for both forward and reverse propagation.

For the forward dynamic mode, the fields have basically the same transverse distribution as in the lossless case studied in [13]–[15]. Here, also, the rate of decay of the fields away from the ferrite and dielectric slabs increases with frequency. The dielectric slab is, in this case, thin enough so as not to modify substantially the field distribution from that of a ferrite slab alone. It was also confirmed that the dynamic-mode structure is "quasi-TEM" with $H_z$ very much smaller than $H_x$ for frequencies up to at least 8 GHz.

The surface (magnetostatic) mode has been discussed in earlier publications [13]–[15] and is not materially changed.

The higher order modes in the lossless case have a cutoff frequency at the intersection with the line $\omega = \beta c_0/\sqrt{\epsilon_d}$ in the $\omega$-$\beta$ diagram. To the left of this line, no nonradiating modes could exist. However, in the problem treated here, losses are taken into account, and the dispersion diagrams corresponding to the higher order modes not only continue to the left of the line $\omega = \beta c_0/\sqrt{\epsilon_d}$ but also attain a slope greater than the velocity of light. This is not surprising since, in the case of

a lossy medium, the group velocity $d\omega/d\beta$ no longer gives the velocity of propagation of the energy. Instead, this is given by the rate of energy flow, determined by the Poynting vector and divided by the stored energy density of the wave [23].

The field distributions for the points on the left of the line $\omega = \beta c_0/\sqrt{\epsilon_d}$ are not essentially different from the ones at the right of this line. But now it can hardly be said that most of the energy propagates within or in the vicinity of the ferrite and dielectric slabs, for the rate of decay of the fields in the semi-infinite dielectric region (region 3) is rather low.

Transverse field distributions for the dynamic and first-order modes for the case of Figs. 2 and 3 can be found in [24].

We are now ready to analyze in detail the results obtained in terms of the effect of each parameter on the behavior of our model. For the sake of simplicity and concreteness we have chosen to retain as fixed throughout this study the saturation magnetization ($4\pi M_s = 1760$ G) and the dielectric constant ($\epsilon_f = 15$) of the ferrite, as well as the dc magnetizing field ($H_0 = 200$ Oe). The effects on the $\omega$-$\alpha$ and $\omega$-$\beta$ diagrams produced by each one of the various parameters involved in this problem will be discussed next.

### A. The Conductivity $\sigma$

When $\sigma$ is high (100 mho/m or more) we observe an absorption peak in the neighborhood of the frequency $f_0 + f_m$, as shown in Fig. 4, where we present the attenuation constants for different values of $\sigma$, as well as a sample dispersion curve. Little change is observed in this characteristic as $\sigma$ changes except for the one feature discussed below.

At $f = f_0 + f_m$ the real part of the ferrite effective permeability $\mu_{\text{eff}}$ is zero, and its imaginary part is small and negative. The wave impedance inside the ferrite slab, therefore, will become small at this frequency, thus approaching a short circuit. Hence, near the frequency $f_0 + f_m$ the magnitude of the electric field in the vicinity of the ferrite–dielectric interface decreases so that the energy is now more evenly distributed throughout the ferrite volume, and, therefore, the effect of the lossy region becomes dominant. We can expect, then, an increase in the attenuation constant in the vicinity of $f_0 + f_m$. For a more detailed discussion of this feature, see [24]. The perturbation of the $\omega$-$\beta$ diagram at $f \sim f_0 + f_m$ is due to computational inaccuracy. This effect occurs only for $\sigma \geq 1000$ mho/m.

The results obtained for $\sigma \geq 100$ mho/m cannot be considered as useful for the study of a nonreciprocal device, because of the high forward insertion loss within the range of utilization of the dynamic mode.

Acceptable results are obtained when $\sigma$ is allowed to take values between 1 and 10 mho/m because its effect on the insertion loss for the forward direction is not

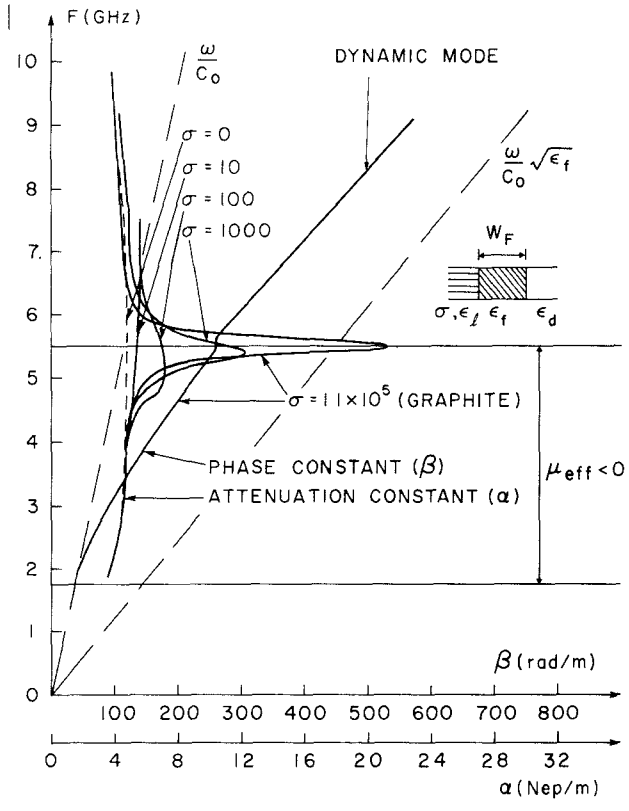


Fig. 4. Dynamic-mode attenuation constant as a function of the frequency for different values of the conductivity of the lossy region. Forward propagation. The $\omega$-$\beta$ diagram for the case of $\sigma = 1.1 \times 10^5$ mho/m is included. Parameters: $4\pi M_s = 1760$ G, $H_0 = 200$ Oe, $\Delta H_0 = 90$ Oe, $W_F = 10$ mm, $\epsilon_f = 15$, $\epsilon_l = \epsilon_d = 1$.

significant. In fact, for frequencies away from the interval where the absorption peak occurs for high conductivities, it was observed that the insertion loss is rather independent of $\sigma$. The insertion loss is mostly controlled by the ferrite linewidth $\Delta H_0$, the dielectric constant of region 2 (the dielectric slab), and the dielectric constant of region 1 (the lossy region), as will be seen later in this section. In the reverse direction, the effect of $\sigma$ on the dynamic-mode attenuation constant dominates [see Figs. 2, 3, and 5, 6].

### B. The Ferrite Resonance Linewidth $\Delta H_0$

The linewidth $\Delta H_0$ is the loss parameter of the ferrite, and, therefore, its effect will not depend on the exact nature of the transverse field distribution. For the reverse dynamic mode, its effect is to enhance the attenuation constant (isolation). In the forward direction, it sensibly controls the insertion loss.

### C. Width $W_D$ and Dielectric Constant $\epsilon_D$ of the Dielectric Slab (Region 2)

An increase in both or either $\epsilon_D$ or $W_D$ would lower the onset of the first higher order mode, thus diminishing the effective operating band of any device employing the dynamic mode. On the other hand, an increase in $\epsilon_D$

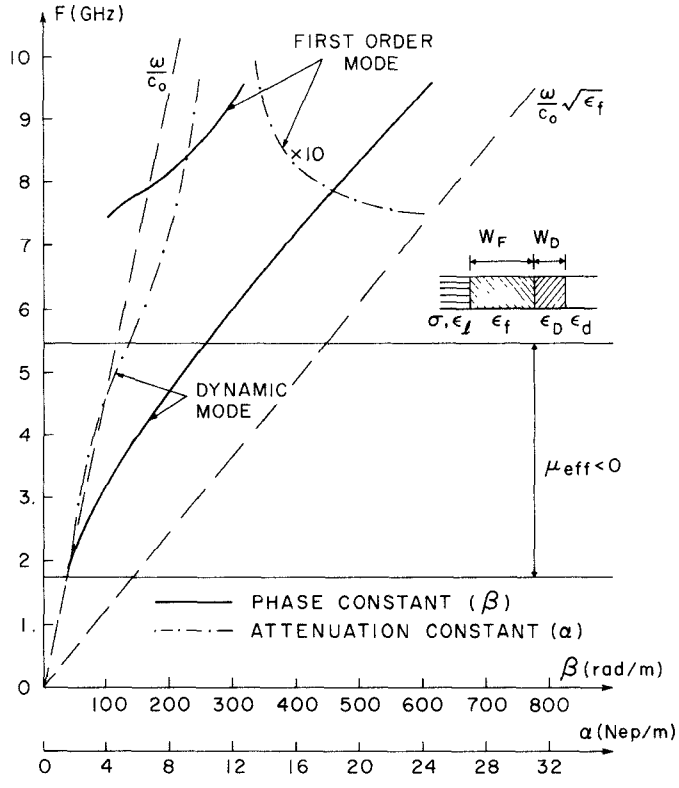


Fig. 5. Dispersion characteristics and attenuation constants for the optimum design. Forward propagation. Parameters: $4\pi M_s = 1760$ G, $H_0 = 200$ Oe, $\Delta H_0 = 45$ Oe, $\sigma = 1.5$ mho/m, $W_F = 7$ mm, $\epsilon_f = 15$, $W_D = 0$, $\epsilon_D = \epsilon_d = 1$, $\epsilon_l = 15$.

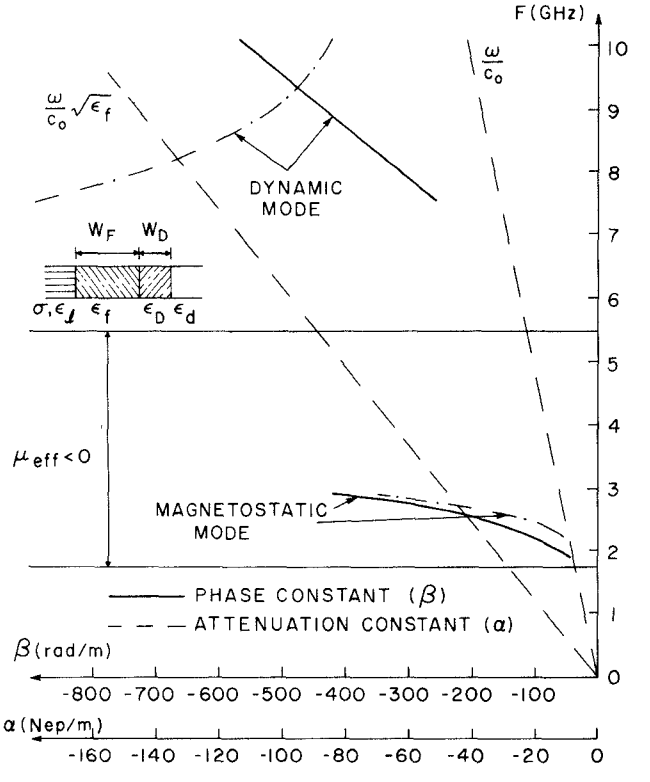


Fig. 6. Dispersion characteristics and attenuation constants for the reverse propagation. Parameters as for Fig. 5.

would lower the insertion loss because, in the forward dynamic mode, more energy is pulled away from the lossy region towards the dielectric slab thus reducing the influence of the lossy material.

Although not shown here, varying the width $W_D$ has an effect on the forward attenuation constant at the lower end of the band. The case $W_D = 2$ mm (when $W_F = 10$ mm) proved to be optimum in the sense of giving an almost flat attenuation constant curve, as can be seen in Fig. 2. We also observe that for $W_D = 0$ the behavior is close to the one observed in Fig. 4 at the lower end of the band. This is so because, as has been mentioned before, the insertion loss can be considered to be independent of $\sigma$ for frequencies above and below those for which the absorption peak occurs.

### *D. The Ferrite Slab Width $W_F$*

Throughout these calculations a slab width of $W_F = 10$ mm was used. When $W_F$ is reduced, the onset of the first higher order mode is delayed. On the other hand, the insertion loss would be increased since the energy, which for the forward direction is concentrated near the interface opposite to the lossy region, now interacts more strongly with the lossy region.

### *E. The Dielectric Constant $\epsilon_l$ and $\epsilon_d$ of the Lossy Material and Semi-Infinite Dielectric Region (Region 3), respectively*

When $\epsilon_l$ is low (of order 1), these two parameters do not have an evident influence on the overall behavior of our model. When $W_D \to 0$ the arguments with respect to $\epsilon_D$ now apply to $\epsilon_d$.

When $\epsilon_l$ takes high values, that is, of the order of $\epsilon_f$ or more, it was observed that it exerted a considerable influence on both the insertion loss and the isolation. Fig. 5 shows that the insertion loss at the upper end of the band increases because as the frequency increases the energy shows a tendency to be more evenly distributed throughout the ferrite (see [13]–[15], [24]. It can then be expected that since the high permittivity lossy region will tend to attract more energy, its effect will be more evident at the upper end of the band, thus increasing the insertion loss.

With regard to the isolation, the same reasoning applies, i.e., a higher $\epsilon_l$ will tend to concentrate the energy near the lossy region, thus increasing the attenuation. Surprisingly enough, however, for fixed $\epsilon_l$, an increase in $\sigma$ causes a decrease in the isolation and vice versa. This unexpected behavior is also advantageous, for a lower $\sigma$ will result in a somewhat lower insertion loss and a higher isolation. It must be noted, however, that a lower $\sigma$ also lowers the first-order mode attenuation constant, and, therefore, a compromise must be attained.

An optimum design of an isolator employing this model is presented next. We chose Yttrium Garnet G-113 from Trans-Tech with characteristics very similar to the ones

used throughout this study:

$$4\pi M_s = 1780 \text{ G}$$
$$\epsilon_f = 15\,\epsilon_0$$
$$\Delta H_0 = 45 \text{ Oe}.$$

For this design to be closely related to our foregoing study, the bias magnetization was taken to be $H_0 = 200$ Oe as before. With these specifications the design was considered to be optimum in the sense of giving minimum insertion loss and maximum isolation for the widest frequency band for the following values of the parameters involved: $W_F = 7$ mm, $W_D = 0$, $\epsilon_d = 1$, $\epsilon_D = 1$, $\epsilon_f = 15$, $\sigma = 1.5$ mho/m. The corresponding characteristic diagrams are shown in Fig. 5 and 6.

We must now assume a length for our hypothetical isolator, so as to be able to express the isolation and insertion loss in decibels instead of nepers per meter. The results presented in this way will allow comparison with those obtained by other authors. Assume then that the length is $l = 2$ cm. Lengths of the same order were employed, for example, by Hines [2] and Dydyk [19] in their prototypes.

By examining Fig. 5 we see that due to the influence of the high $\epsilon_f$ the insertion loss is highest at the upper end of the band where its value is approximately 0.8 dB/cm. The forward first-order mode has an attenuation of over 20 dB (10 dB/cm or 130 Np/m on the graph) for frequencies up to 10 GHz.

On the other hand, from the reverse characteristic we observe that at 10 GHz the isolation is approximately 15 dB (85 Np/m or 7.4 dB/cm). It was not possible to find the first-order mode for the reverse direction, and we can safely assume that it will be at least as attenuated as is the case for forward propagation. The magnetostatic mode is, in turn, not sufficiently attenuated (>20 dB) except for frequencies above, approximately, 3 GHz.

Hence, our isolator has the following characteristics:

| | |
|---|---|
| range | 3–10 GHz |
| bandwidth | 1 2/3 octaves |
| isolation | $\geqslant$ 15 dB |
| insertion loss | $\leqslant$ 1.6 dB. |

Hines, using the same ferrite material for an isolator 1 in (2.5 cm) long, obtained an insertion loss better than 2 dB and an isolation greater than 15 dB over a range from 7 to 9.75 GHz, approximately.

Dydyk presents two isolators with different kinds of dissipative loading for a ferrite of $4\pi M_s = 1000$ G. For his film loaded ($R_s = 268\ \Omega$/sq) component, the experimental isolation reported is greater than 15 dB while the maximum insertion loss is 1.7 dB for a band from 2 to 8 GHz (two octaves). For the bulk-loaded isolator the isolation is better than 23 dB over two octaves (2–8 GHz) and better than 15 dB from 2 to 12 GHz. The insertion loss is less than 2.4 dB in the 2–12-GHz range.

Forterre *et al.* report the development of several isolators for different frequency ranges. Two of these operate in a band nearly equivalent to that of our model. Their characteristics are, for the first one ($4\pi M_s = 1000$ G): range 2–10 GHz, insertion loss $\leqslant$ 1.5 dB, isolation $\geqslant$ 15 dB; and for the second one ($4\pi M_s = 1780$ G): range 3.5–14 GHz, insertion loss $\leqslant$ 1.0 dB, isolation $\geqslant$ 20 dB.

In comparing these experimental results with ours, it must be remembered that a ferrite with a much lower resonance linewidth would give a lower forward insertion loss. The first of the prototypes above employs a ferrite with a linewidth of 5 Oe, whereas the value used in our optimization was 45 Oe. Yet, the insertion loss measured is close to that of our calculated result which, besides, neglected copper loss.

With regard to the work described by Forterre *et al.*, some differences were found between the dispersion diagram given in [17] and those that appear here which deserve comment. For the forward dynamic mode, they observe that it has a cutoff at the intersection with the line $\omega = \beta c_0$, whereas in the case of our work we have seen that the dynamic mode is always a zero cutoff mode. The reason for this is that Courtois' model considers a vertical perfect magnetic wall at the edge of the conducting strip, which causes the dynamic mode to have a cutoff at $f = \sqrt{f_0(f_0 + f_m)}$. (See [5]–[7].)

The $\omega$-$\beta$ diagram presented in [17] also shows a cutoff for the first-order mode at the intersection with the line $\omega = \beta c_0$, even though the problem studied takes losses into account. However, it has become clear from our results that the higher order modes may extend into the region to the left of this line when losses are introduced. The extremely high loss in this region will quench these modes quite effectively, and, therefore, they cannot play a significant role.

## IV. Conclusion

The results of a detailed study of the modal spectrum for a configuration modeling the inhomogeneously ferrite-loaded stripline, subjected to a magnetizing field directed normal to the ground planes, have been presented. A four-region model consisting of a slab of ferrite between two infinite perfectly conducting planes loaded with both a semiinfinite lossy material and a dielectric slab at opposite faces was treated.

A detailed study on how the various parameters involved affect the behavior of the model was conducted. The model has been shown to be qualitatively as well as quantitatively in good agreement with experimental results of isolators developed by Hines, Dydyk, and Courtois.

In comparing our results with those of Forterre *et al.* reported in [17], we have pointed out the differences between the two models. It has become clear that, due to the presence of loss mechanisms, the higher order modes extend to the left of the line $\omega = \beta c_0/\sqrt{\epsilon_d}$ and do not have a cutoff at the intersection with this line.

More detailed studies would require the inclusion of the fringing fields in our modeling of the homogeneously and inhomogeneously ferrite-loaded striplines (Bolle [13] and deSantis [25]) as well as possibly the conductor losses. Conductor losses have previously been considered by Courtois [16], [17]. In addition, our program allows the obtaining of data concerning nonreciprocal phase shifters by suitably modifying the geometric configurations considered here.

## References


[1] M. E. Hines, "A new microstrip isolator and its application to distributed diode amplification," in *IEEE G-MTT, 1970 Int. Microwave Symp. Dig. Paper*, Newport Beach, CA, pp. 304–307.

[2] ——, "Reciprocal and nonreciprocal modes of propagation in ferrite stripline and microstrip devices," *IEEE Trans. Microwave Theory Tech.*, vol. MTT-19, pp. 442–451, May 1971.

[3] ——, "Ferrite transmission devices using the edge-guided mode of propagation," in *IEEE G-MTT, 1972 Int. Microwave Symp. Dig. Papers*, Chicago, IL, pp. 236–237.

[4] P. deSantis and R. Roveda, "Magnetodynamic boundary waves," in *Proc. Europ. Microwave Conf.*, Stockholm, Aug. 23–28, 1971, pp. C5/2:1–C5/2:4.

[5] L. Courtois, G. Declercq, and M. Peurichard, "On the non-reciprocal aspect of gyromagnetic surface waves," presented at the Seventh Annual Conf. on Magnetism and Magnetic Materials, Chicago, IL, Nov. 16–19, 1971; in *Seventh Annual Conf. on Magnetism and Magnetic Materials, Proc.* part 2, pp. 1541–1545, AIP, 1972.

[6] L. Courtois, "Propagation Oblique des ondes electromagnétiques dans une lame de ferrite aimantée parallelement a ses faces," *Electronica y Fisica Aplicada*, vol. 16, no. 2, pp. 286–294, 1973.

[7] L. Courtois, B. Chiron, and G. Forterre, "Propagation dans une lame de ferrite aimantée: Application a de noveaux dispositifs non reciproques a large bande," *Cables et telecommunications*, no. 4, pp. 417–435, Oct. 1973.

[8] G. Cortucci and P. deSantis, "Edge-guided waves in lossy ferrite microstrips," in *Proc. 1973 Europ. Microwave Conf.*, Brussels, vol. 2, p. B9–1.

[9] P. deSantis, "Edge-guided modes in ferrite microstrip with curved edges," *Appl. Phys.* (Springer-Verlag, Germany), vol. 4, no. 2, pp. 167–174, Aug. 1974.

[10] ——, "A unified treatment of edge-guided waves," NRL Rep. 8158, Naval Research Laboratory, Washington, DC, Jan. 27, 1978.

[11] D. M. Bolle, "The edge-guided mode on ferrite loaded stripline," in *1976 IEEE-MTT-S Int. Microwave Symp. Dig.*, pp. 257–259, June 1976.

[12] ——, "The peripheral or edge-guided modes on the inhomogeneously and homogeneously ferrite loaded stripline," in *Sixth Europ. Microwave Conf. Dig.*, Rome, Italy, pp. 560–564, Sept. 1976.

[13] ——, "A study of ferrite loaded planar waveguiding structures," Tech. Rep. N00014-75-C-0750/1, Division of Engineering, Brown University, Providence, RI, Mar. 1977.

[14] ——, "The modal spectrum of ferrite-loaded striplines," *1977 IEEE MTT-S Int. Microwave Symp. Dig.*, pp. 519–522, June 1977.

[15] ——, "The modal spectrum of ferrite-loaded striplines, II," *Seventh Europ. Microwave Conf. Dig.*, Copenhagen, Denmark, Sept. 1977.

[16] L. Courtois, G. Forterre, and B. Chiron, "Improvement in broad band ferrite isolators," in *Proc. Twentieth Conf. on Magnetism and Magnetic Materials*, p. 501, 1974.

[17] G. Forterre, B. Chiron, and L. Courtois, "A survey of broad band stripline ferrite isolators," *IEEE Trans. Magn.*, vol. MAG-11, Sept. 1975.

[18] L. Courtois, N. Bernard, B. Chiron, and G. Forterre, "A new edge-mode isolator in the very high frequency range," *IEEE Trans. Microwave Theory Tech.*, vol. MTT-24, Mar. 1976.

[19] M. Dydyk, "Edge-guide: One path to wideband isolator design," Parts I–II, in *Microwaves*, pp. 55–58, Jan. 1977; pp. 50–56, Feb. 1977.

[20] IMSL Library 1 (for IBM 370/360 Series). See IMSL Library Manual.

[21] K. M. Brown, "A quadratically convergent Newton-like method based upon Gaussian elimination," *SIAM J. on Numerical Analysis*, vol. 6, no. 4, pp. 560–569, 1969.

[22] K. M. Brown and J. E. Dennis, Jr., "On the second order convergence of Brown's derivative-free method for solving simultaneous nonlinear equations," Yale University Dept. of Comput. Sci. Tech. Rep., pp. 71–77, 1971.

[23] R. Loudon, "The propagation of electromagnetic energy through an absorbing dielectric," *J. Phys. A: Gen. Phys.*, (Great Britain), vol. 3, 1970.

[24] S. H. Talisa and D. M. Bolle, "A study of ferrite loaded planar waveguiding structures, II," Tech. Rep. N00014-75-C-0750/2, Division of Engineering, Brown University, Providence, RI, May 1978.

[25] P. deSantis, "Fringing-field effects in edge-guided wave devices," *IEEE Trans. Microwave Theory Tech.*, vol. MTT-24, no. 7, July 1976.